VSP

Journal of Adhesion Science and Technology 24 (2010) 2499–2510

Journal of ADHESION SCIENCE and TECHNOLOGY
brill.nl/jast

Theoretical and Experimental Study of the Influence of AFM Tip Geometry and Orientation on Capillary Force

Alexandre Chau [a], **Stéphane Régnier** [b], **Alain Delchambre** [a] **and Pierre Lambert** [a,*]

[a] BEAMS Department, Université libre de Bruxelles, CP 165/56, 1050 Bruxelles, Belgium
[b] ISIR, 4 Place Jussieu BP 173, 75252 Paris Cedex 05, France

Abstract
Adhesion issues are present in many disciplines such as, for example, surface science, microrobotics or MEMS design. Within this framework, this paper presents a study on capillary forces due to capillary condensation. A simulation tool had already been presented using Surface Evolver and Matlab to compute the shape of a meniscus in accordance with the Kelvin equation and contact angles. The numerical results of this simulation complied well with literature results. One very important result is the ability to compute the evolution of the capillary force depending on the tilt angle of the gripper with respect to the object. The main contribution of this new paper is a test bench and the related experimental results which validate these numerical results. We present here new experimental results illustrating the role of humidity and tilt angle in capillary forces at the nanoscale.

Keywords
Condensation, capillary forces, adhesion, AFM, tilt angle, Kelvin equation

1. Introduction

When considering applications at small scale, adhesion cannot be ignored. For example, capillary adhesion is important in micromanufacturing [1] or in assembly of small components [2]. Contrary to marco-world ruled by gravity, small scale applications are governed by surface forces. Indeed, when size diminishes and the objects are scaled down, surface forces become more important and the major opposing force to picking up and releasing micro- and nanocomponents becomes the force of adhesion [3]. The force needed to separate two objects is also known as pull-off force. Adhesion can also prevent structures like RF-MEMS or any high aspect ratio structures from normal functioning [4].

The adhesion force is actually composed of different components: electrostatic force, van der Waals force, chemical forces and capillary force. Electrostatic

* To whom correspondence should be addressed. E-mail: pierre.lambert@ulb.ac.be

 DOI:10.1163/016942410X508307

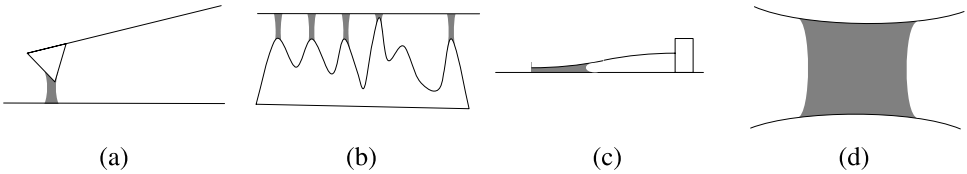

Figure 1. Some case studies in which capillary condensation can occur: (a) adhesion between an AFM tip and a substrate; (b) capillary bridges between roughness asperities and a — rough or not — substrate; (c) stiction of a cantilevered beam, and (d) scheme of the problem tackled in this work (two solids S_1 and S_2 are linked by a capillary bridge. Besides geometry, the main parameters of this problem are the contact angles made by the liquid on S_1 and S_2, surface tension γ of the liquid and the surrounding humidity).

force can be avoided by choosing materials properly (conductive materials to avoid charge accumulation and similar junction potentials to avoid a capacitive effect between two objects brought close to one another). Van der Waals force arises from the intrinsic constitution of matter: it is due to the presence of instantaneous dipoles. It becomes non-negligible at the nanometer scale. Chemical forces are due to the bondings between objects. It is active when objects are in contact (i.e., the distance between them is about an intermolecular distance).

Capillary force between two objects is due to the presence of liquid between them (see Fig. 1). It has already been shown [5, 6] that it can be used to manipulate submillimetric objects (with 300–500 μm characteristic dimension) by manually placing a liquid droplet on the object (a fraction of μl). At nanoscale, the liquid comes from capillary condensation of ambient moisture.

This nanomanipulation will require force modulation, in order to pick up and release components: the picking force should be larger than the other forces while the force applied on the component during release should be lower than its weight or any other adhesion force. It is proposed here to control the force by tilting the tip (an application could be an AFM tip) with respect to the object. Models which assume objects and meniscus to be axially symmetrical [7, 8], therefore, become inapplicable. A more general model thus has been developed to compute the capillary force without this constraint of axisymmetry.

We already published in [9] a theoretical study aiming at assessing the use of capillary force as a picking principle. The main result of this theoretical study is reproduced with permission in this new paper (Fig. 4), but the main contribution of this new paper consists in experimental results on capillary forces at the nanoscale.

This paper is organized as follows: first, the basic equations will be recalled (Section 2), and their validity discussed. Our simulation tool will then be presented (Section 3.1) together with some theoretical results (Section 3.3). The section on experimental study presents the experimental details and setup used in this work (Section 4.1) and the results are presented in Section 4.2. After discussion in Section 5, conclusions are drawn in Section 6.

2. Model

2.1. Introduction

This section details the different equations involved in the problem description: (i) the Kelvin equation [3, 10], which governs the curvature of the liquid meniscus according to environmental parameters (humidity and temperature), and (ii) the approaches encountered in the literature to compute the capillary force, i.e., the Laplace approach and the energetical approach (based on the derivation of the total surface energy U_S). Both methods are presented in our previous work [9] but the first method is not convenient for 3D-geometries (i.e., non-axially symmetric geometries) and will, therefore, not be presented in this work anymore.

In all cases, gravity is neglected, i.e., the meniscus height h is so small that the hydrostatic pressure difference $\rho g h$ is much smaller than the capillary pressure: this is the case for $h \ll 1$ mm.

2.2. Kelvin Equation

In any method used to compute the capillary force, the meniscus shape appears explicitly or implicitly. In the Kelvin equation approach, the meniscus geometry is involved through the total mean curvature H of the meniscus, or its inverse r, the mean curvature radius:

$$H = \frac{1}{r} = \frac{1}{2r_K} = \frac{1}{2}\left(\frac{1}{r_1} + \frac{1}{r_2}\right), \tag{1}$$

where r_K is, in the case of capillary condensation, the so-called Kelvin radius, and r_1 and r_2 are the two principal curvature radii. The Kelvin radius is governed by the Kelvin equation [3, 10] which is the fundamental equation for capillary condensation. It links the curvature of the meniscus with environmental and materials properties:

$$r_K = \frac{\gamma V_m}{RT \log_e(p/p_0)}, \tag{2}$$

where V_m is the molar volume of the liquid, R is the gas constant (8.31 J/mol K), T the temperature (in Kelvin) and p/p_0 is the relative humidity (RH), between 0 and 1. Typically, for water, this gives $r_K = 0.54 \text{ nm}/\log_e(\text{RH})$, which gives for RH = 90%, a Kelvin radius of about 5 nm at 20°C.

2.3. Energetical View

The total energy of the meniscus can be expressed as:

$$U_S = \gamma_{LV} A_{LV} + \gamma_{LO} A_{LO} + \gamma_{LT} A_{LT} + \gamma_{OV} A_{OV} + \gamma_{TV} A_{TV}, \tag{3}$$

where γ_{ij} is the interfacial tension of the i–j interface: Liquid, Vapor, Object and Tip, and A_{ij} are the areas of these interfaces.

The capillary force in the z-direction can then be computed using a classical derivative of the energy with respect to the distance between the objects. If the

problem is axisymmetrical, the z-direction is the axis of symmetry, otherwise it can be any direction along which the force is calculated. Note that the energy is derivatized with respect to the separation distance z to obtain the capillary force in the direction of this separation, but according to [11], it must be emphasized whether the derivative is done assuming constant volume of liquid or constant pressure. In the case of constant volume of liquid, de Boer and de Boer [11] give for the force (positive is taken to be attractive):

$$F(z) = \frac{\mathrm{d}U_{\mathrm{S}}}{\mathrm{d}z}, \tag{4}$$

while in the case of constant pressure:

$$F(z) = \frac{\mathrm{d}U_{\mathrm{S}}}{\mathrm{d}z} - \frac{\gamma}{r_{\mathrm{K}}}\frac{\mathrm{d}V}{\mathrm{d}z}. \tag{5}$$

In this work, according to de Boer and de Boer [11], before separation, the initial condition for the capillary volume will be established by the Kelvin radius. Then, the constant volume assumption will be used since it is reported by de Boer and de Boer that the force–distance curve is rate-independent for withdrawal times from 0.01 to 10 s, which is typically the case in this work. In other words, withdrawal times are short enough to guarantee that the liquid does not evaporate. This point will be discussed later on in the next subsection.

2.4. Validity of the Equations

Both methods presented here are based on macroscopic assumption on the nature of the liquid and solids: matter is continuous and so are its properties such as surface tension. It has been shown experimentally that the Kelvin equation is valid down to menisci of radii in the range 4–20 nm for cyclohexane condensed between mica surfaces [12] and in the range 5–65 nm for water [13]. For smaller radii, the discrete nature of matter should be taken into account, *via* molecular dynamics or Monte-Carlo calculations [14]. The results will thus have to be interpreted keeping in mind that their validity is not proven for very small sizes of meniscus (i.e., for menisci with radii <4 nm).

Another question raised by the literature is the parameter which is kept constant during derivatization: should the latter be computed keeping the volume or the curvature constant [15]? Different mechanisms play a role here, mainly the condensation/evaporation rate. It seems that the condensation takes place on the millisecond (<5 ms [15]) scale while the evaporation needs more time. It has been measured that meniscus stretching at tip-object distance is much larger than r_{K}. Capillary condensation also has a long term (up to tens of days) component, which will not be considered here [16].

If experimental investigation could provide an estimation of the characteristic times involved in the processes, it would seem natural to compute the volume condensed — fulfilling the Kelvin equation — at the smallest tip-object distance and

then compute the evolution of the force with constant volume when retracting the tip (equation (4)).

3. Numerical Study

3.1. Simulation Tool

The numerical model already presented in [9] is able to cope with non-axisymmetrical menisci, based on the energetical approach described previously. The solver makes use of the software Surface Evolver (SE) [17] to compute the meniscus shape and henceforth to compute equation (3). The base of Surface Evolver is the evolution of a surface toward a local minimum of energy, representing the surface of the meniscus with triangularized mesh. If needed, the mesh can be evolved and refined until satisfactory result is found. The meniscus shape is consequently found by energy minimization, fulfilling both the Kelvin equation on the shape of the meniscus and the contact angles. This solver can be freely downloaded (http://www.susqu.edu/brakke/evolver/evolver.html) and is well documented. In equation (4) we replace the derivative by a finite difference:

$$\frac{\mathrm{d}U_\mathrm{S}}{\mathrm{d}z} = \frac{U_\mathrm{S}(z_i + \Delta z) - U_\mathrm{S}(z_i)}{\Delta z}, \tag{6}$$

where $U_\mathrm{S}(z_i + \Delta z)$ and $U_\mathrm{S}(z_i)$ are computed with Surface Evolver. All computations have been first tested on a personal computer before being batched on the computing cluster Hydra of the Université libre de Bruxelles. (Hydra — the HPC cluster at the VUB/ULB Computing Centre.)

3.2. Available Shapes

To develop complex shapes without having to define each point of the tip (or the object), analytical shapes have been used. In the xz plane (see Fig. 2), usual profiles can be chosen: circular, conical or parabolical, while in the (x, y) plane, the section of the tip can be described as a polar function.

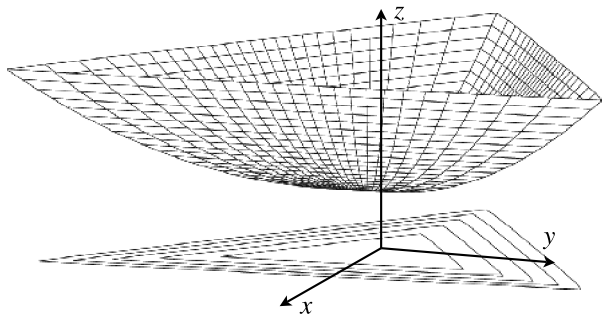

Figure 2. Example of a tip and its projection on the (x, y) plane. Here, the section is a triangle and the profile is a parabola. (Reproduced with permission from [9] © 2007 IEEE.)

Elementary sections are:

- Circle: $r(\theta) = R$;
- Triangle: $r(\theta) = c/(2\sqrt{3}\cos\theta)$ for $-\pi/3 < \theta \leqslant \pi/3$;
- Square: $r(\theta) = c/(2\cos\theta)$ for $-\pi/4 < \theta \leqslant \pi/4$.

In a similar way, any regular polygon of side length c can be very easily implemented. Actually, virtually any section can be represented as it is developed in Fourier series (in polar coordinates) in order to obtain an analytical shape in the domain $\theta = [0; 2\pi]$.

The profile and section are then coupled to obtain the complete tip that has to be used in the equations. An example of a tip with parabolic profile and triangular section is shown in Fig. 2. Such a geometrical description can also be applied to the object.

3.3. Theoretical Results

3.3.1. Introduction

The results presented in this section are twofold. First, validity of the code is shown in Section 3.3.2. As literature provides results only for axisymmetrical shapes, those results will be the only ones that can be used as a proof for the model, since no results are available for other shapes.

Then, in Section 3.3.3, more complex shapes will be investigated (effects of tip tilting).

3.3.2. Validation

In [8], analytical solutions are derived from the base equations. They provide results for the sphere–plane and sphere–sphere cases separated by a liquid bridge. The results (see Fig. 3) are presented with respect to the so-called filling angle [3], which is the angle defining the position of the triple line on the sphere (measured from the vertical axis). One can see that the correspondence is very good with the model from [8] and that the approximation of [3] ($F = 4\pi R\gamma\cos\theta$) is valid for very small filling angles.

The discrepancies between the model results and [8] can be explained by the meshing of the meniscus. The mesh refinement has to be limited to keep the computation time acceptable. In general, the total computation time for a configuration is in the 1–5 min range.

In [7], the shape of the tip is a parabola. The force values are also in good agreement as shown in [9]. Results in [18] and [19] have also been used as benchmarks.

3.3.3. Tilted Tips

One main feature of our model is its ability to compute non-axisymmetrical tips. Therefore, we presented in [9] the influence of the tilt angle τ on the force for a conical tip (see Fig. 4).

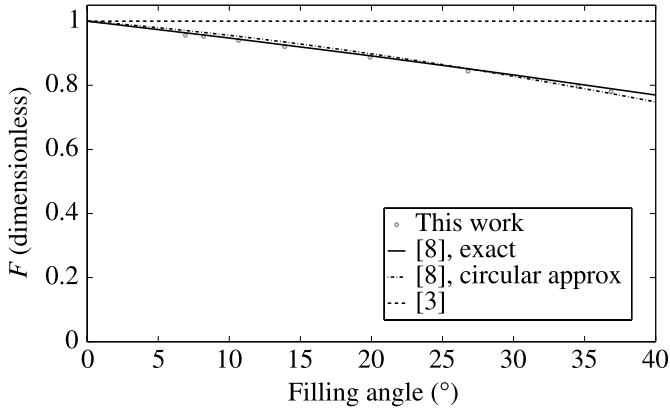

Figure 3. Comparison of normalized capillary force F (dimensionless) at the contact between a sphere and a plane for several models ($\theta_1 = \theta_2 = 40°$). The positive value of force means an attractive force. (F is the force divided by the quantity $2\pi R(\cos\theta_1 + \cos\theta_2)$, the filling angle is the angle defined by the arc of the sphere which joins the triple line to the contact point.)

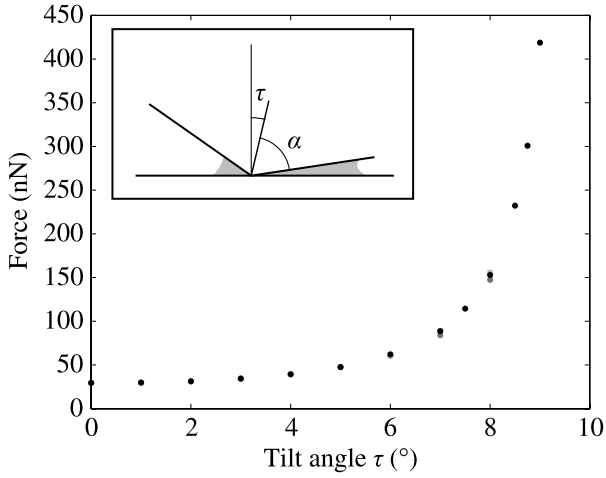

Figure 4. Force between a tilted tip (the tilt angle is τ) and a plane. The aperture angle of the cone (α) is 80°, temperature is 298 K, the relative humidity is 90%. Both contact angles are 30° and the surface tension is 72 mN/m. The positive value of force means an attractive force. The different points at the same tilt angle are for different mesh refinements. They give an idea of the numerical uncertainty in the results. The enclosed sketch defines the aperture angle of the cone α and the tilt angle τ. (Reproduced with permission from [9] © 2007 IEEE.)

The conical tip for which the results are presented has an aperture angle α of 80° (the tilt angle is thus limited to a maximum of 90–80 = 10°). One can see that the force can vary from about 30 nN to over 400 nN, simply by tilting the tip over the plane. This principle is expected to serve as a basis to modulate the capillary force and hence to allow micro/nanomanipulation of components.

4. Experimental Study

4.1. Experimental Test Bench

In order to validate the model, a test bench has been developed, following an AFM type design (see Fig. 5): a Thorlabs CPS198 laser (detail 1) is reflected by an AFM tip (detail 4) onto a Pacific Silicon Sensor QP50-6SD2 photodiode (detail 7), using lenses (details 3–6) and mirrors (details 2–5). When a force is applied on the AFM tip, the tip is deflected, changing the direction of the reflected beam. This modification can be measured using the photodiode. The laser spot displacement on the photodiode can then be converted to a force since the tip has a known stiffness (about 0.8 N/m).

Currently, the force can be measured between an AFM tip and a substrate placed in an environmental box (Fig. 6, detail 9). The substrate can be moved vertically over a 25 mm range with a 200 nm resolution (with a PI M-126 translation stage), and over a further 200 μm range with a 1 nm resolution (with a PI P-528 nanopositioning system, detail 8).

The tip and substrate (mica, used 30 min after cleavage, is assumed to be atomically flat) are approached until contact, then the pull-off force is measured when retracting the substrate. (Silicon tips were supplied by Nanoandmore. They have a nominal stiffness $k_m = 0.8$ N/m, and two different curvature radii of 90 nm and 150 nm: they have been modelled as elliptical tips.) As the tip and the substrate can be enclosed in a small environmental box, humidity can be controlled and the

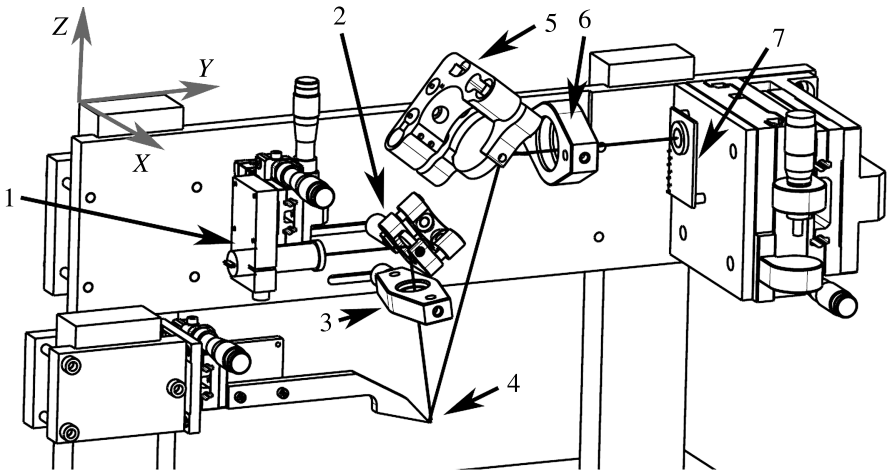

Figure 5. Test bench developed: the solid line indicates the optical path of the laser beam emitted from (1), reflected by a mirror (2) and passing through a lens (3) before being reflected by a cantilever (4). The reflected beam is sent towards a second mirror (5) before passing through a second lens (6) and illuminating a photodiode (7) whose voltage output is a measure of the beam deflection. Knowing the stiffness of the cantilever, this voltage output can be converted into a force with a resolution of the order of 10 nN.

variations of the force with respect to humidity can be measured. A typical pull-off measurement has already been presented in [9].

The sources of error are the quality of substrate and tip surfaces, the stiffness uncertainty (estimated from the cantilever thickness a 10% uncertainty for the range (0.75–1.40) $\times$ k_m), electrical noise, positioning stages precision, and contact detection variability. The temperature variation effects can be ignored since only a variation of 0.03° has been registered during a 30-min experiment. All these errors contribute to the experimental scatter depicted in Fig. 7.

4.2. Experimental Results

The model presented in this article computes only the capillary component of the adhesion force, while experimental results include all other effects (van der Waals and electrostatic forces). In order to compare model results with experimental ones, we chose to vary a parameter that had an effect only on capillary force.

The most relevant parameter meeting this criterion is relative humidity. Indeed, the assumption that relative humidity has only minor impact on other forces than capillary force is acceptable. The variation of the capillary force with respect to relative humidity can thus be computed and experimentally measured.

In Fig. 7, different batches of pull-off measurements have been made with varying RH. A least squares fit is then made on the points. It is shown as a dashed line. For the same geometry, computations have been made, and the results are given by

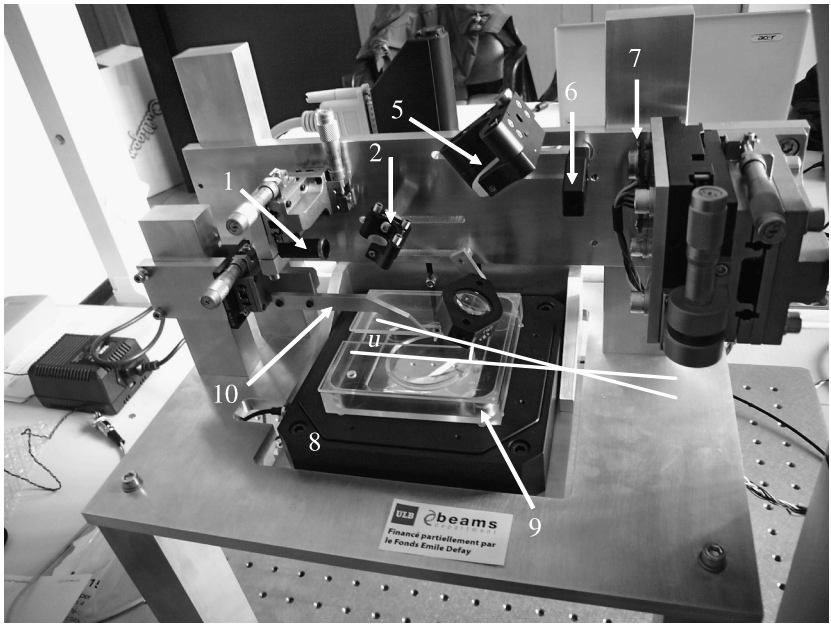

Figure 6. In addition to Fig. 5, we can see in this figure the nano-positioning stage (8), the environmental box (9) and the part on which the cantilever is glued (10). The angle u is the angle between the substrate to be placed on the bottom of the environmental box and the cantilever (4, not shown here).

the solid line. (As already said, only the slope of these curves is to be observed, i.e., the dependence on humidity.) The simulation gives a slope of 0.23 nN/% while the best fit leads to a slope equal to 0.27 nN/% with a standard deviation equal to 0.035 nN/%. In these simulations the contact angles have been assumed close to zero since they cannot be measured at this scale.

Similarly, the measurements and computations of Fig. 7 have been done for different tip to substrate tilt angles. The results are shown in Fig. 8. Results quali-

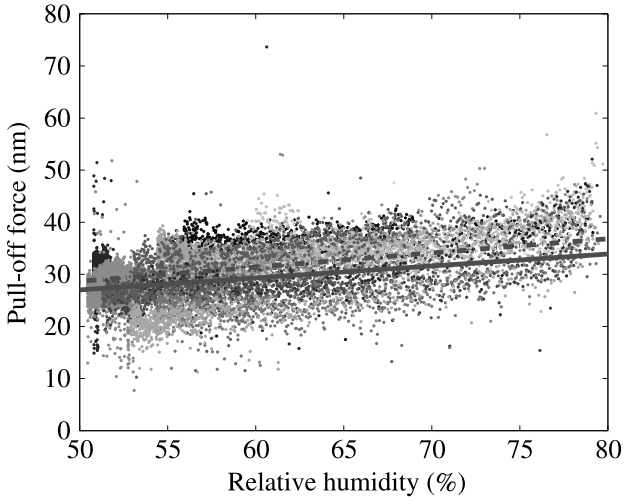

Figure 7. Force measurements: for different humidities, the pull-off force has been measured. The dashed line is the linear regression of the measurement points. The solid line is the result of the model.

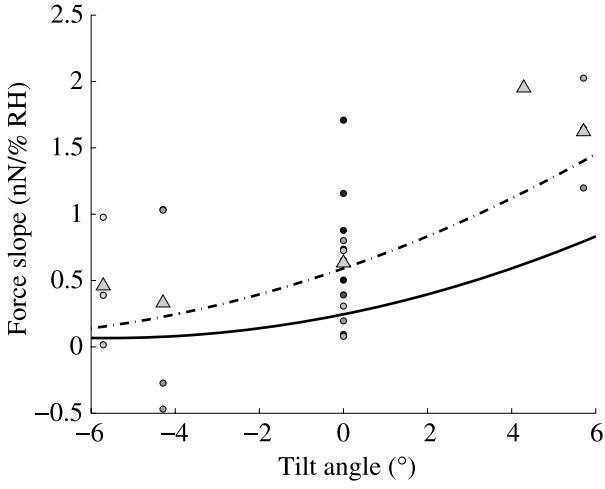

Figure 8. Slope of the pull-off force *vs* humidity with respect to the tilt angle. For each tilt angle, the mean is given by the triangles. The 4th triangle must be treated with care as it is based on a single batch. The solid line is the result of the model; the dot-dashed line is the result of the model for a 4° tilt bias because this 4° tilt deviation is assumed to be a measure for the uncertainty in the initial value of the angle u. It is shown for sensitivity demonstration purpose.

tatively fit but a significant deviation can be observed. One assumption is that there is an error in the angle u between the tangent to the mica substrate placed on the bottom of the environmental box (Fig. 6, detail 9) and the cantilever which is glued on the holding part (Fig. 6, detail 10). This error can come from different sources: glueing of the cantilever on the holding part, manufacturing and assembly errors in the chain linking the holding part to the environmental box, alignment error between the bottom of the box and the mica substrate. This error cannot be measured easily in our setup, consequently we decided to study the sensitivity of the capillary force to this angle parameter u. To do so, the environmental box was tilted with respect to the reference horizontal orientation. The capillary force as a function of this tilt angle (i.e., variation of u) is plotted in Fig. 8.

5. Discussion

In the previous paragraphs, it was shown that our model could be used to compute the capillary force between two objects for usual shapes: spheres, cones, planes... and reproduce existing results. In addition, the three-dimensional capabilities of the model allow the user to compute capillary force for complex configurations with simple shapes or even with complex shapes (e.g., pyramids, rounded pyramids that can model the Berkovich AFM tips).

Results presented in Figs 7 and 8 show fair agreement between experimental and theoretical measurements. Different sources of measurement noise were identified out of which the main one was the surface modification. To overcome the scatter, we repeated the measurements to be able to have statistical results. Another method to limit the scatter could be to work with atmospheres of controlled composition, not just humidity control.

A very interesting result presented is that the force can be varied using tip tilting. This should allow the user to pick up and release a part by controlling the tilt angle of the tip with respect to the object.

To give the order of magnitude, a force of about 50 nN is sufficient to lift a cube of about 280 μm for a density of 2300 kg/m^3 (approximately the density of silicon). For objects with such masses, a tip should be able to pick up, manipulate, and then release them.

The manipulable part weights can also be extended using different tip shapes or using multiple tips.

6. Conclusions

This paper presents a three-dimensional model for the computation of the capillary force, allowing to compute the effects of capillary condensation, with configurations that are not mandatorily axisymmetrical. The model has been validated by comparing it with existing theoretical results. The model was also compared to experimental results using a dedicated test bench. The comparison has shown a fair

correspondence even if the quantitative correlation is arguable. Experiments under controlled atmosphere could improve measurements.

It was shown here that the tilt angle of a tip with respect to a flat substrate is an important parameter to vary the capillary force between them. This result is promising for a new application in micromanipulation of components. Nevertheless, experiments are going on to determine how to make use of this effect with better repeatability.

Acknowledgement

This work has been funded by a grant from the *F.R.I.A. — Fonds pour la Formation à la recherche dans l'industrie et l'agriculture*.

References

1. D. Wu, N. Fang, C. Sun and X. Zhang, *Sensors Actuators A* **128**, 109–115 (2006).
2. C. H. Mastrangelo, *J. Microelectromechanical Syst.* **2**, 33–43 (1993).
3. J. N. Israelachvili, *Intermolecular and Surface Forces*, 2nd edn. Academic Press (1992).
4. T. Kondo, S. Juodkazis and H. Misawa, *Appl. Phys. A* **81**, 1583–1586 (2005).
5. P. Lambert and A. Delchambre, *Langmuir* **21**, 9537–9543 (2005).
6. P. Lambert, F. Seigneur, S. Koelemeijer and J. Jacot, *J. Micromech. Microeng.* **16**, 1267–1276 (2006).
7. T. Stifter, O. Marti and B. Bhushan, *Phys. Rev. B* **62**, 13667–13673 (2000).
8. F. M. Orr, L. E. Scriven and A. P. Rivas, *J. Fluid Mech.* **67**, 723–742 (1975).
9. A. Chau, S. Régnier, A. Delchambre and P. Lambert, in: *Proceedings of IEEE International Symposium on Assembly and Manufacturing*, pp. 215–220 (2007).
10. A. W. Adamson and A. P. Gast, *Physical Chemistry of Surfaces*, 6th edn. Wiley (1997).
11. M. P. de Boer and P. C. T. de Boer, *J. Colloid Interface Sci.* **311**, 171–185 (2007).
12. L. R. Fisher and J. N. Israelachvili, *Colloids Surfaces* **3**, 303–319 (1981).
13. M. M. Kohonen and H. K. Christenson, *Langmuir* **16**, 7285–7288 (2000).
14. J. Jang, M. A. Ratner and G. C. Schatz, *J. Phys. Chem. B* **110**, 659–662 (2005).
15. L. Sirghi, R. Szoszkiewicz and E. Riedo, *Langmuir* **22**, 1093–1098 (2005).
16. F. Restagno, L. Bocquet and T. Biben, *Phys. Rev. Lett.* **84**, 2433–2436 (2000).
17. K. Brakke, *Expl. Math.* **1**, 141–165 (1992).
18. A. de Lazzer, M. Dreyer and H. J. Rath, *Langmuir* **15**, 4551–4559 (1999).
19. O. H. Pakarinen, A. S. Foster, M. Paajanen, T. Kalinainen, J. Katainen, I. Makkonen, J. Lahtinen and R. M. Nieminen, *Model. Simul. Mater. Sci. Eng.* **13**, 1175–1186 (2005).